SDC-92-378

SDC
SOLENOIDAL DETECTOR NOTES

TRIPLET COINCIDENCE IN DRIFT TUBES FOR A LEVEL 1 MUON TRIGGER

November 30, 1992

A.T.M. Wang
University of South Carolina

Triplet Coincidence in Drift Tubes for a Level 1 Muon Trigger

A.T.M. Wang
University of South Carolina
and Superconducting Super Collider Laboratory

November 30, 1992

Abstract

This note investigates a conceptual Level 1 single track Muon trigger based on triplet drift tube coincidences in superlayers. Such a trigger could provide a stand-alone timing circuit within a projective angular range of ± 16 deg without trigger scintillators, and with a time resolution that permits matching the track with a particular beam crossing. The geometrical acceptance is independent of p_t for a projective geometry, and the geometrical efficiency for calculating a single track solution is 100 percent for all angles.

1 Introduction

The calculation of the absolute time-of-arrival of particles passing through three layers of a drift detector is further developed in this note. We study the coincidences between the two overlapping contiguous triplets of a four element superlayer (Figure 1), and briefly describe the non-contiguous triplets, and the coincidences between triplets in separate superlayers. A triplet coincidence algorithm, by its nature, incorporates data from an offset layer to correctly resolve the left-right ambiguity of drift directions and the related large-angle/small angle ambiguity (see Figure 2) that cause misidentification of low momentum tracks as high momentum tracks[2, 4]. In addition, a trigger signal based on coincidences between triplets can achieve a timing resolution sufficient to resolve the beam crossings without additional trigger scintillators.

2 Equations for Contiguous Triplets

In Figure 1 a single straight muon track passes through two superlayers of a muon drift tube system (e.g. BW2 and BW3 superlayers in the SDC barrel muon system). Superlayer

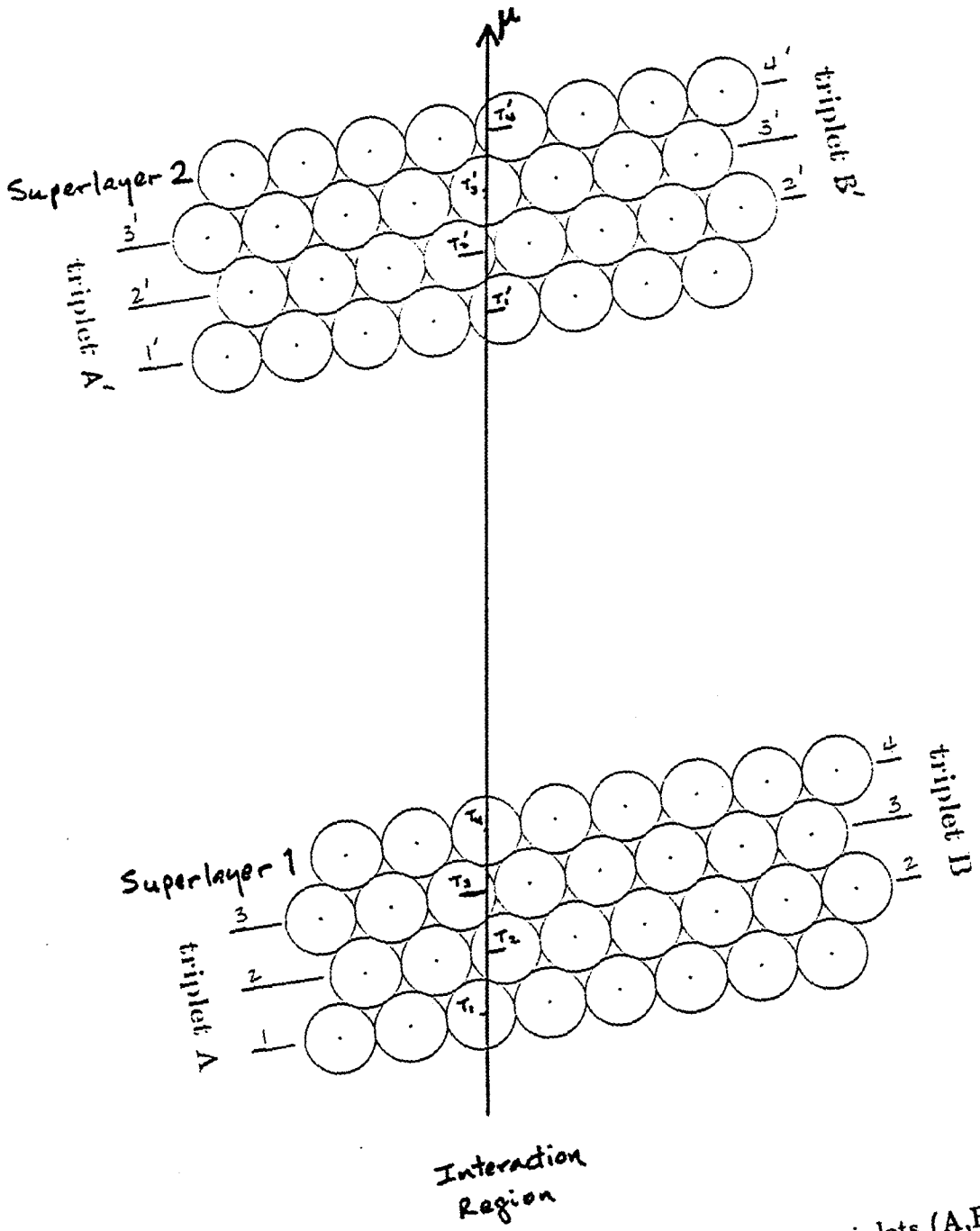

Figure 1: Single high p_t muon passing though overlapping triplets (A,B) and (A',B') in superlayers BW2 and BW3

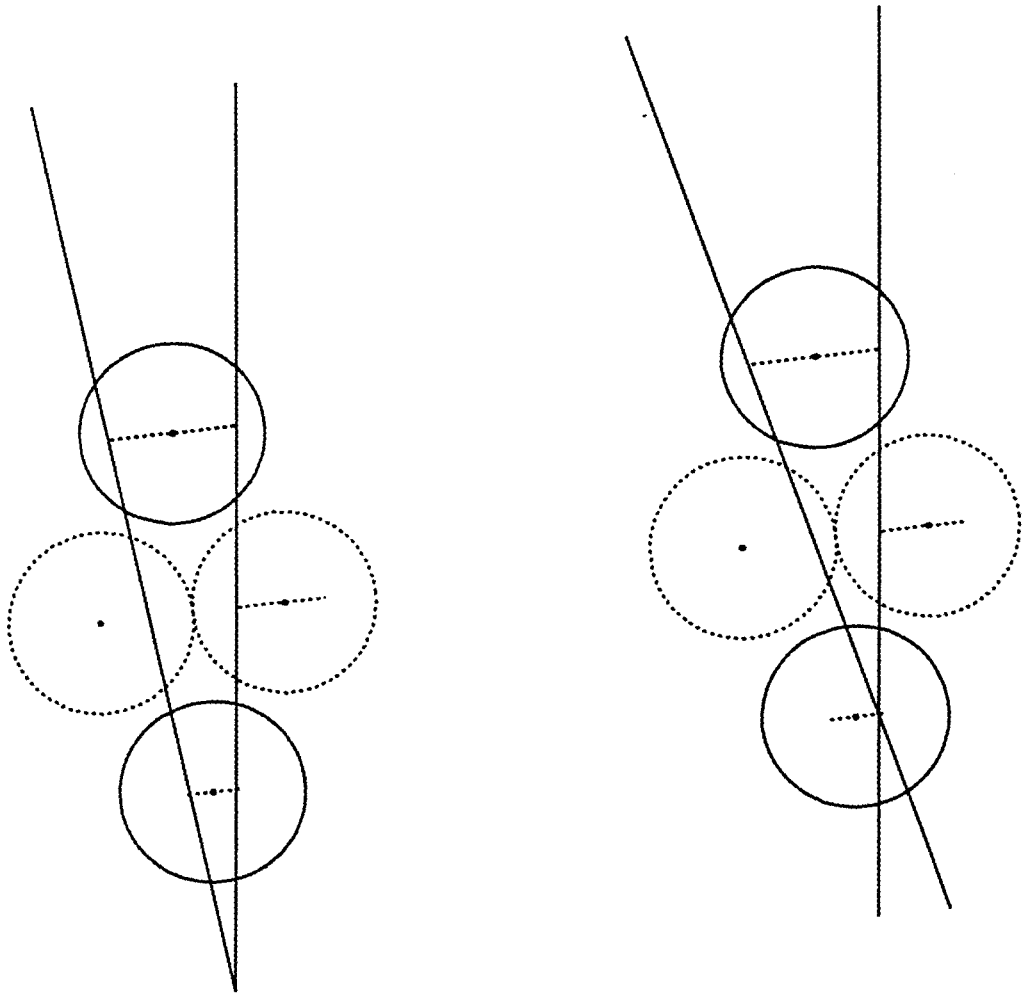

Figure 2: Consequences of drift direction ambiguity in drift tubes pairs. In each case the ambiguity is resolved by the offset third layer. (a) Left-right ambiguity, (b) Large-angle/small-angle ambiguity

1 (BW2) contains the two overlapping triplets, A and B. The composite signals W1, W2, W3 and W4 come from a hard-wire OR of the anode wires in their respective layers. For the purpose of this study, we assumed 100% efficiency in all tubes and zero thickness for the tube walls and anode wires. Straight tracks were generated through the muon superlayers at angles from −60 to +60 deg and in 1 mm steps from −90 to +90.

Figure 3 shows the idealized geometry of close packed tubes with alternate layers offset by a half-cell that we used in our calculations for both SDC-type and GEM-type drift tube configurations. The results are similar and can be parametrized in terms of the radius, layer spacing and critical angle ϕ_c. (The critical angle is defined to be that of a straight line passing through the anode wires of all three cells in a diagonal stack.) In our previous work [1], we obtained four analytical solutions corresponding to different configurations of track position, incident angle and drift directions in a stack. We now define a new condition for all remaining possible tracks in contiguous triplets.

2.1 Triplet Drift time equations

We shall review the four solutions for the crossing time T_0 derived from drift time information in the muon layers. It will be seen that the time origin for these measurements is arbitrary. Figure 4 shows an idealized time picture of signals generated in layers W1, W2, and W3. We calculate two time differences δt_1, and δt_2 from the arrival times T_1, T_2 and T_3. For each triplet we calculate a variable delay time X in terms of δt_1, δt_2 and T_{tot}. T_{tot} represents a known maximum drift time for charges originating near the drift tube wall to reach the anode wire. The crossing time T_0 is given by $T_{\text{tot}} - X$ which corresponds to the elapsed time from the instant of the muon crossing to the arrival of the signals from all three layers. We define δt_1 to be the time interval between T_2 and the later of T_1 and T_3, and δt_2 to be the time interval between the signals in W1 and W3. That is:

$$\delta t_1 = |T_2 - \max(T_1, T_3)| \quad \text{and} \quad \delta t_2 = |T_1 - T_3| \tag{1}$$

Note that δt_1 provides the auxiliary information needed to resolve the left-right ambiguity, and that δt_2 is proportional to the angle of the track and inversely proportional to p_t. We also invoke the principle of drift time symmetry in the following condition:

$$T_{\text{tot}} = \frac{(T_1 + T_3)}{2} + T_2 \tag{2}$$

In the simplest case, the muon track lies within the boundaries of an imaginary drift tube stack consisting of three vertical half-cells. We then obtain an equation (Solution 1) for the delay interval X:

$$\text{Solution 1}: \quad X_1 = \frac{T_{\text{tot}}}{2} - \left(\frac{\delta t_1}{2} + \frac{\delta t_2}{4}\right) \tag{3}$$

A geometrical derivation of the above equation can be seen in Figure 3.

SDC

Tube diameter	90 mm
Layer spacing	90 mm
Critical angle	27 deg

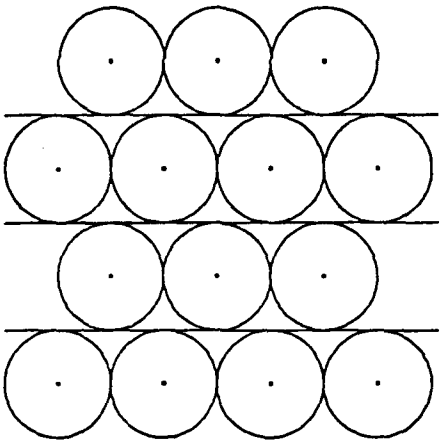

GEM

Tube diameter	40 mm
Layer spacing	34.64 mm
Critical angle	30 deg

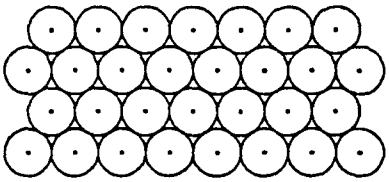

Figure 3: Drift tube configuration for SDC and GEM

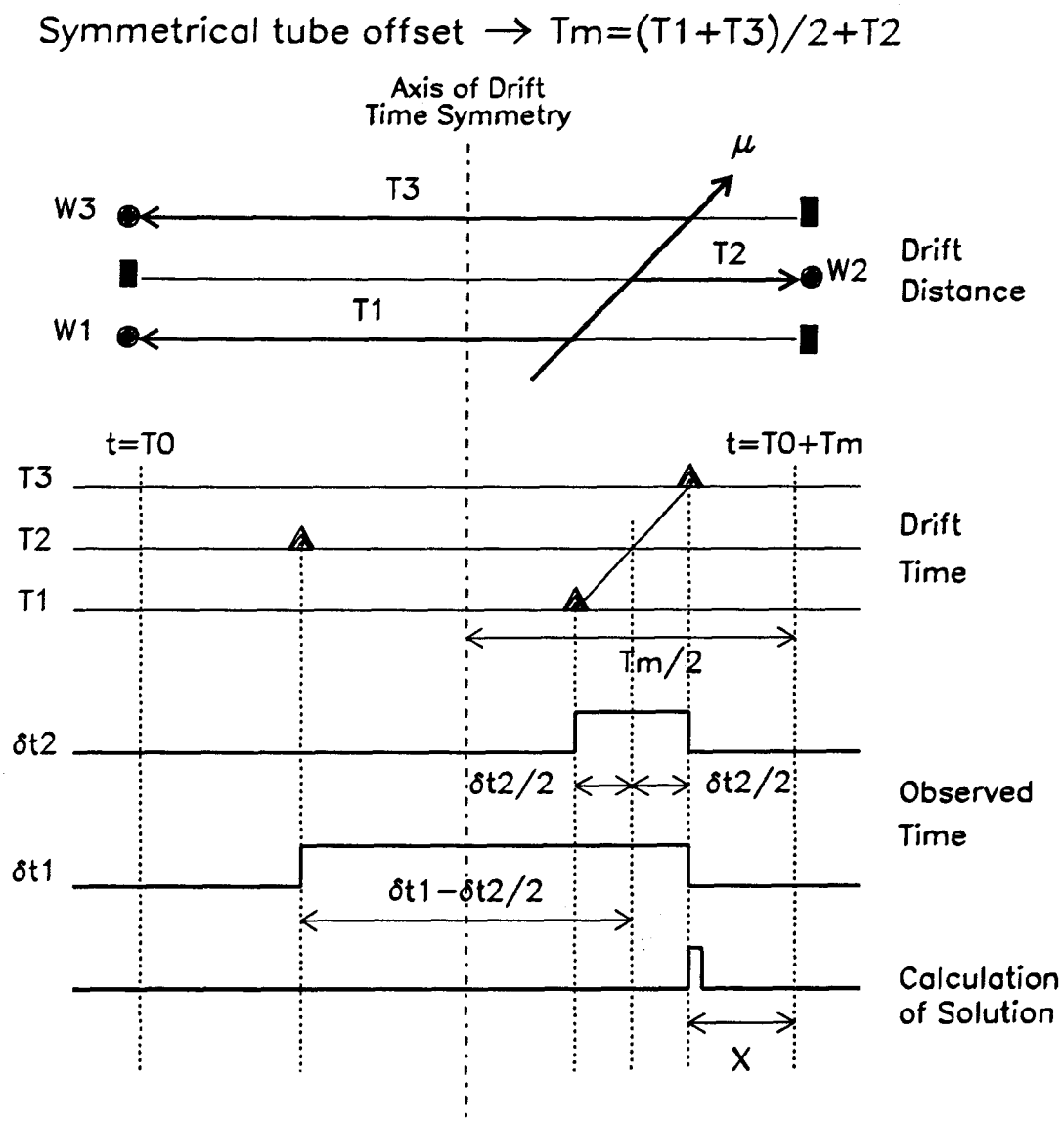

$$X = \frac{Tm}{2} - \frac{(\delta t1 - \delta t2/2)}{2} - \frac{\delta t2}{2} = \frac{Tm}{2} - \left(\frac{\delta t1}{2} + \frac{\delta t2}{4}\right)$$

Figure 4: Geometrical derivation of Solution 1.

However, when the muon track passes outside the boundary of the stack, then Solution 1 is invalid and we obtain three alternate equations (Figure 5), Solutions 2-4, respectively.

$$\text{Solution 2}: \quad X_2 = \frac{\delta t_2}{2} - \delta t_1 \tag{4}$$

$$\text{Solution 3}: \quad X_3 = T_{\text{tot}} - \left(\delta t_1 + \frac{\delta t_2}{2}\right) \tag{5}$$

$$\text{Solution 4}: \quad X_4 = \frac{\delta t_2}{2} \tag{6}$$

Each of the four solutions can be mapped to distinct regions in the 2-dimensional parameter space of track angle ϕ, and impact parameter Y. In our idealized system, the impact parameter is linearly dependent on the drift time. We take Y to be the track position at Layer 1 and ϕ to be the track angle relative to the drift field orientation. It should be noted that although Eqn. 6 is a special case of of Eqn. 4 when $\delta t_1 = 0$, in general $\delta t_1 \neq 0$ when Solution 4 is valid. Figure 6 shows the (Y, ϕ) parameter space regions where solutions 1-4 are valid for triplet A.

In Figure 7(a), all four solutions are shown simultaneously. The empty regions of the parameter space are completely described by the degenerate condition which results when X_2 in Eqn. 4 is equal to zero:

$$\delta t_1 = \frac{\delta t_2}{2}, \tag{7}$$

provided δt_1 and δt_2 are non-zero. These "holes" correspond to tracks where the drift directions are the same in all layers. Since the left-right ambiguity cannot be resolved in this situation, no Solution 5 for X_5 can be found. Figure 7(b) shows the parameter space of this degeneracy condition. In the angular range -14 deg $+14$ deg for SDC and -16 deg to $+16$ deg for GEM the efficiency of obtaining a trigger signal is near unity.

The efficiency of our suggested trigger scheme near the critical angle (30 deg. GEM and 27 deg SDC) may be increased by the use of an additional superlayer without any shifts of the tubes. The critical angle for such a superlayer would equal zero, and the overlap can in principle eliminate the holes in the trigger acceptance.

2.2 Triplet B equations

The same track can satisfy different solutions depending on which combination of three wires is selected. Figure 8 show a track which has no solutions in triplet A ($\delta t_1 = \delta t_2/2$) but which satisfies Eqn 5 in triplet B (valid Solution 3).

The symmetry condition for triplet B is similar to that for triplet A:

$$T_{\text{tot}} = \frac{(T_2 + T_4)}{2} + T_3 \tag{8}$$

and the solutions are identical in form to Eqns. 3-6. Solutions 1-4 for the second triplet are plotted in Figure 9. From the symmetry between triplet A and triplet B, we also expect the general solutions to satisfy the condition: SolutionA(Y, ϕ) = SolutionB(Y $\pm$ nR, ϕ)

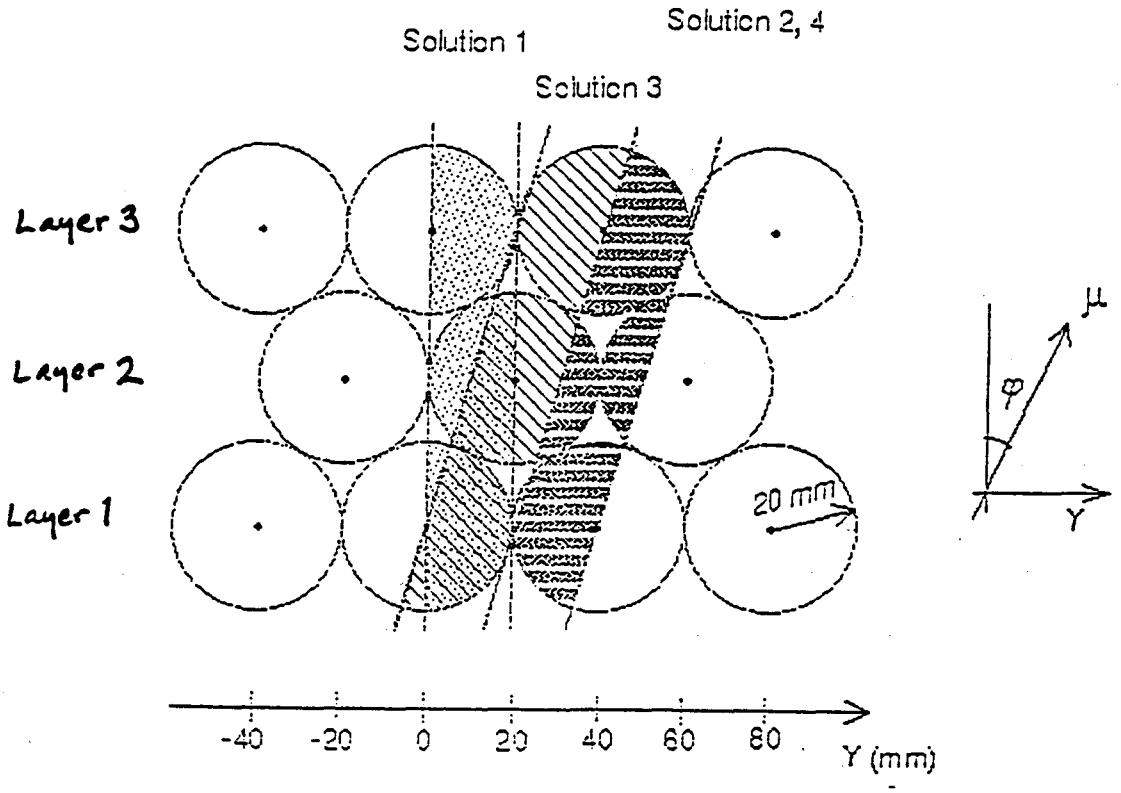

Solution 1: $X_1 = \frac{T_m}{2} - \left(\frac{\delta t_1}{2} + \frac{\delta t_2}{4}\right)$

Solution 2: $X_2 = \frac{\delta t_2}{2} - \delta t_1$

Solution 3: $X_3 = T_m - \left(\delta t_1 + \frac{\delta t_2}{2}\right)$

Solution 4: $X_4 = \frac{\delta t_2}{2}$

Figure 5: Simplified view of drift tube stacks and the corresponding solutions. The track angle has been limited to $0 < \phi < \phi_c$ and the intercept to $0 < Y < 2R$, where R is the radius of the drift cell.

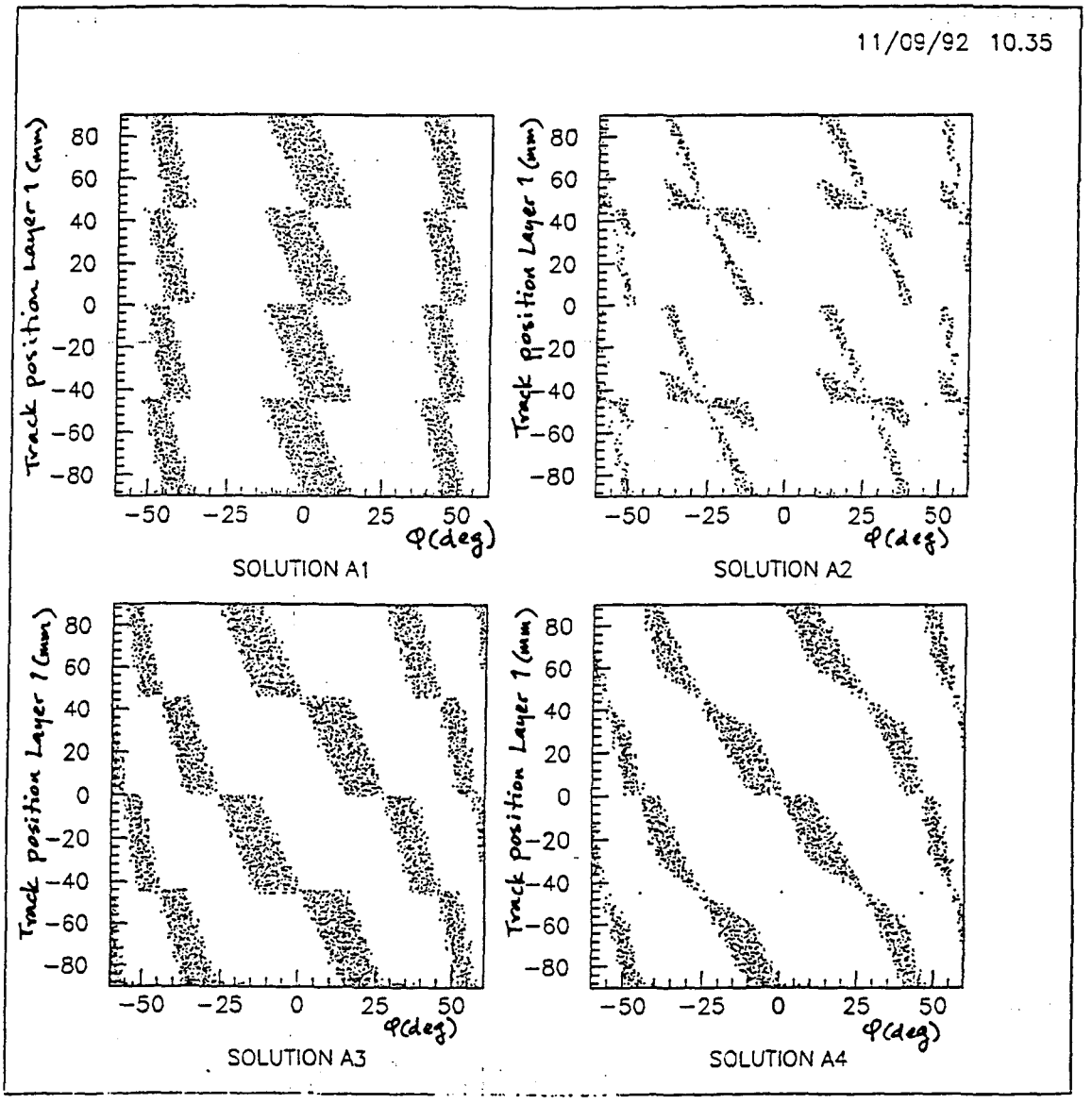

Figure 6: (Y, ϕ) parameter space regions where each Solution gives T0. ϕ is the incident track angle and Y is the position of the track in Superlayer 1.

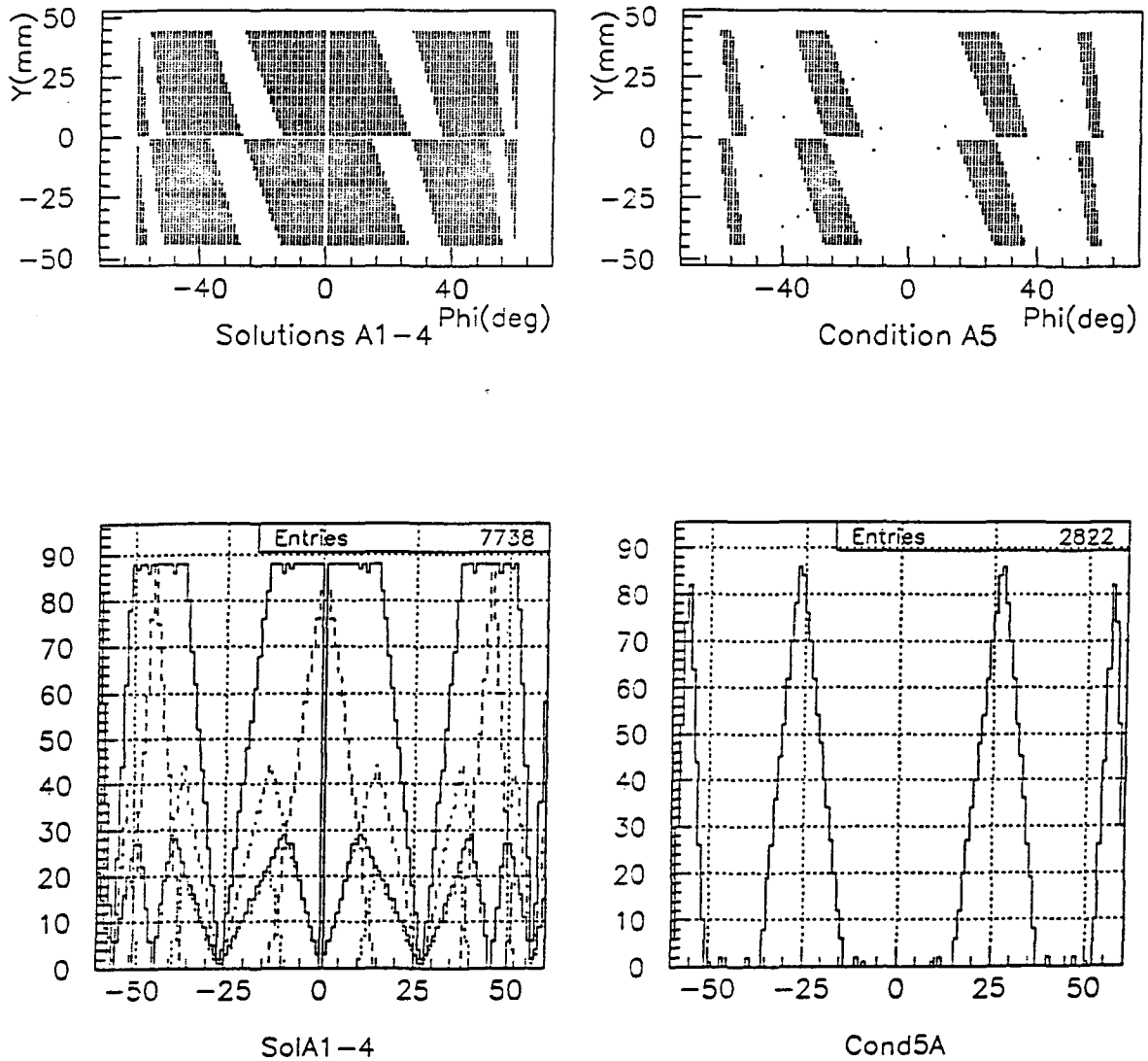

Figure 7: (a) (Y, ϕ) parameter space covered by Solutions A1-4. (b) (Y, ϕ) region where the degenerate condition $t_{1A} = t_{2A}/2$ is valid. (c) Overall angular acceptance of of Triplet A solutions and the separate components. (d) Angular acceptance of degenerate condition.

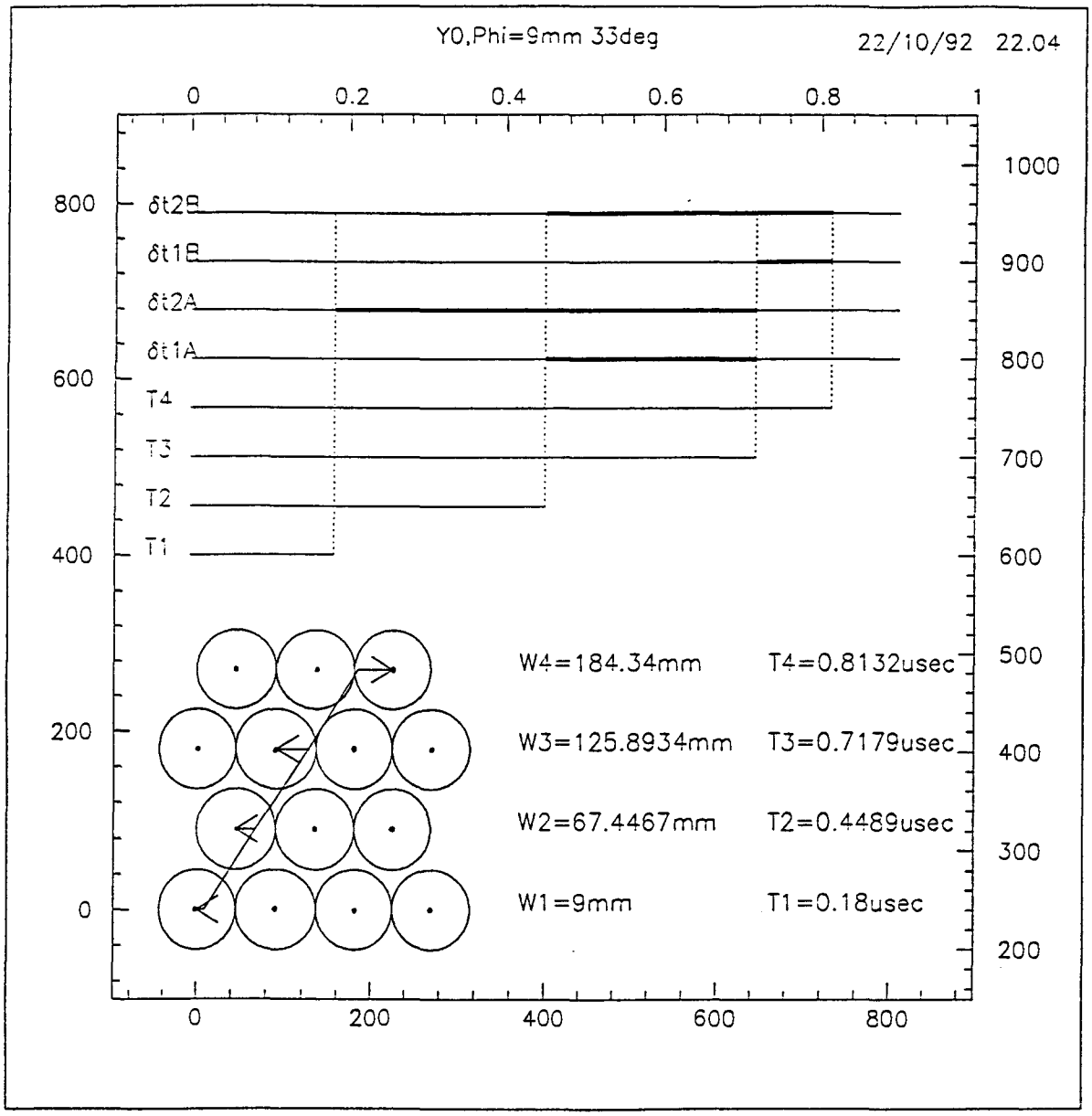

Figure 8: Drift directions for a single track in a superlayer

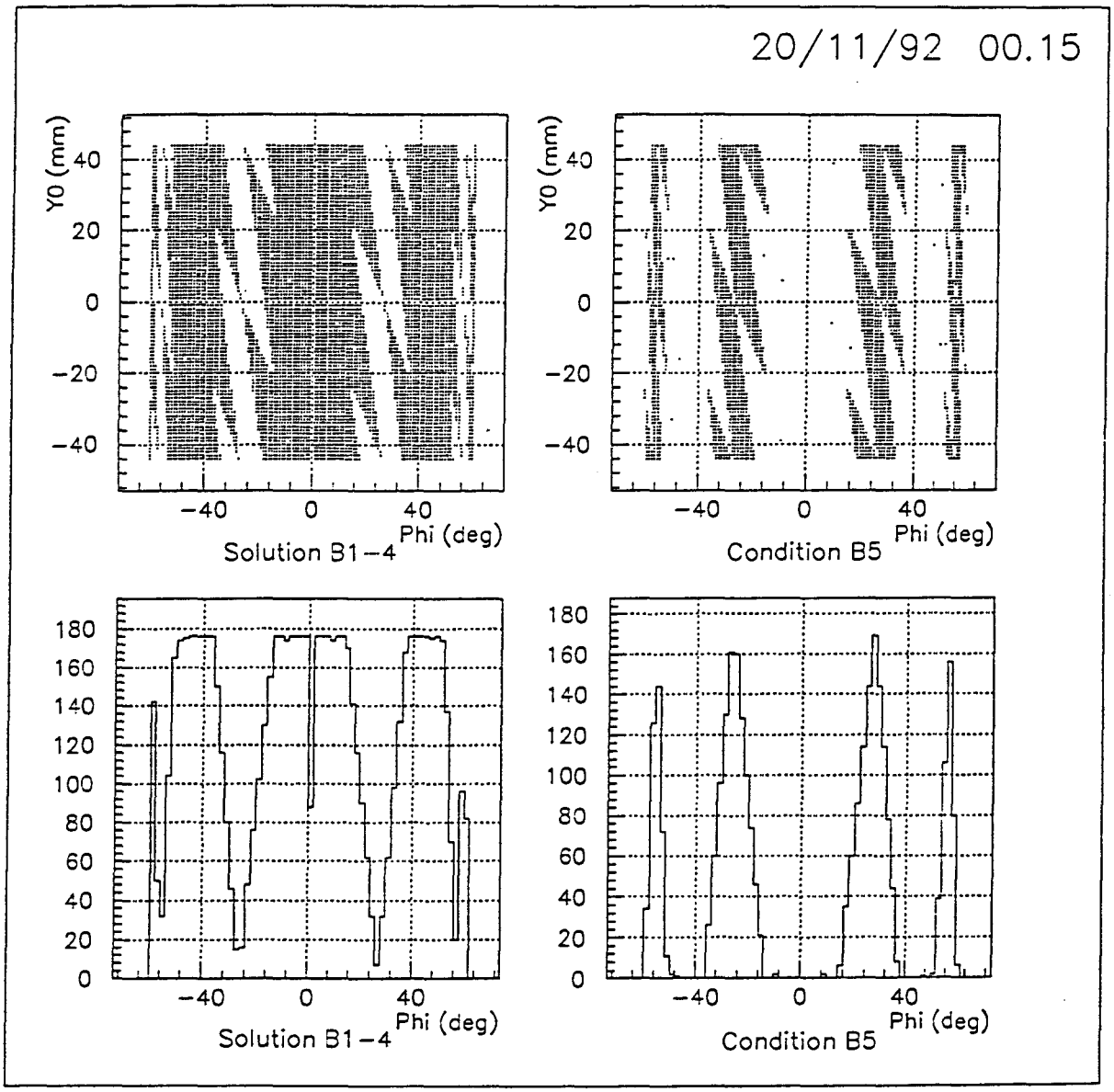

Figure 9: Triplet B ($\phi = 0$ is suppressed.) (a) Solutions B1-4 (b) Degenerate condition (c) Overall angular acceptance (d) Angular range of degenerate condition.

3 Elimination of False Triggers

In any realization of this trigger algorithm, each straight track would generate the five output signals: Sol1, Sol2, Sol3, Sol4 and Cond5, one of which is the true signal and the rest spurious. Identifying the true signal depends on eliminating those false signals which would arrive earlier than the true signal. We have investigated two alternative methods (Figure 10) for reducing the number of false triggers using the drift tube information. The first method uses a complex "OR" of the triplet wire signals (see Figure 5b in Ref. [1]), where the different solutions can be separated at the amplifier stage, and the conditions for rejecting false triggers are shaped after the fast calculation of all four solutions. The second method uses a simple OR and, for the rejection conditions we use linear functions of δt_1 and δt_2 as described below to eliminate irrelevant (A,B) solutions before the fast calculation stage. The two approaches motivate different schematics.

3.1 Rejection after the fast calculation

In the simulation of the complex OR scheme we applied the following set of criteria to the signals (Sol1A, Sol2A, Sol3A, Sol4A) from triplet A, and signals (Sol1B, Sol2B, Sol3B, Sol4B) from triplet B.

Solution 3 is evaluated separately from the other solutions so that a valid Solution 3 blocks other solutions. In addition, there are three rejection criteria within any triplet:

- If $X_2 \leq 0$, then Solution 2 is eliminated,
- If $X_4 = X_2$, then Solution 2 and 4 are eliminated.
- If $\delta t_1 = \delta t_2/2$ when $\delta t_2 \neq 0$, then all Solutions 1,2,3,4 are eliminated.

After the rejection stage, we evaluate the terms: SolA = Sol1A + Sol2A + Sol3A + Sol4A and SolB = Sol1B + Sol2B + Sol3B + Sol4B. and form coincidences MUTR = (SolA * SolB), and MUVT = (Cond5A * Cond5B). MUVT which arises when the degeneracy conditions $\delta t_{1A} = \delta t_{2A}/2$ and $\delta t_{1B} = \delta t_{2B}/2$ are simultaneously true, can be used to block false triggers.

Figure 12 shows the overall efficiency for a single track trigger after the rejection cuts and a 4 nsec wide coincidence of the A-B solutions for $0 \leq \phi \leq 90$ deg. A uniform efficiency of 100% can be seen in the angular range $\phi \leq +18$ deg for the SDC geometry.

3.2 Rejection before the fast calculation

In the Simple OR scheme, we searched for an orthogonal set of conditions that would describe each valid (A,B) combination of solutions. The (A,B) pairs are specified by a linear combination of one or more relations of the four derived time variables ($\delta t_{1a}, ..., \delta t_{2b}$);

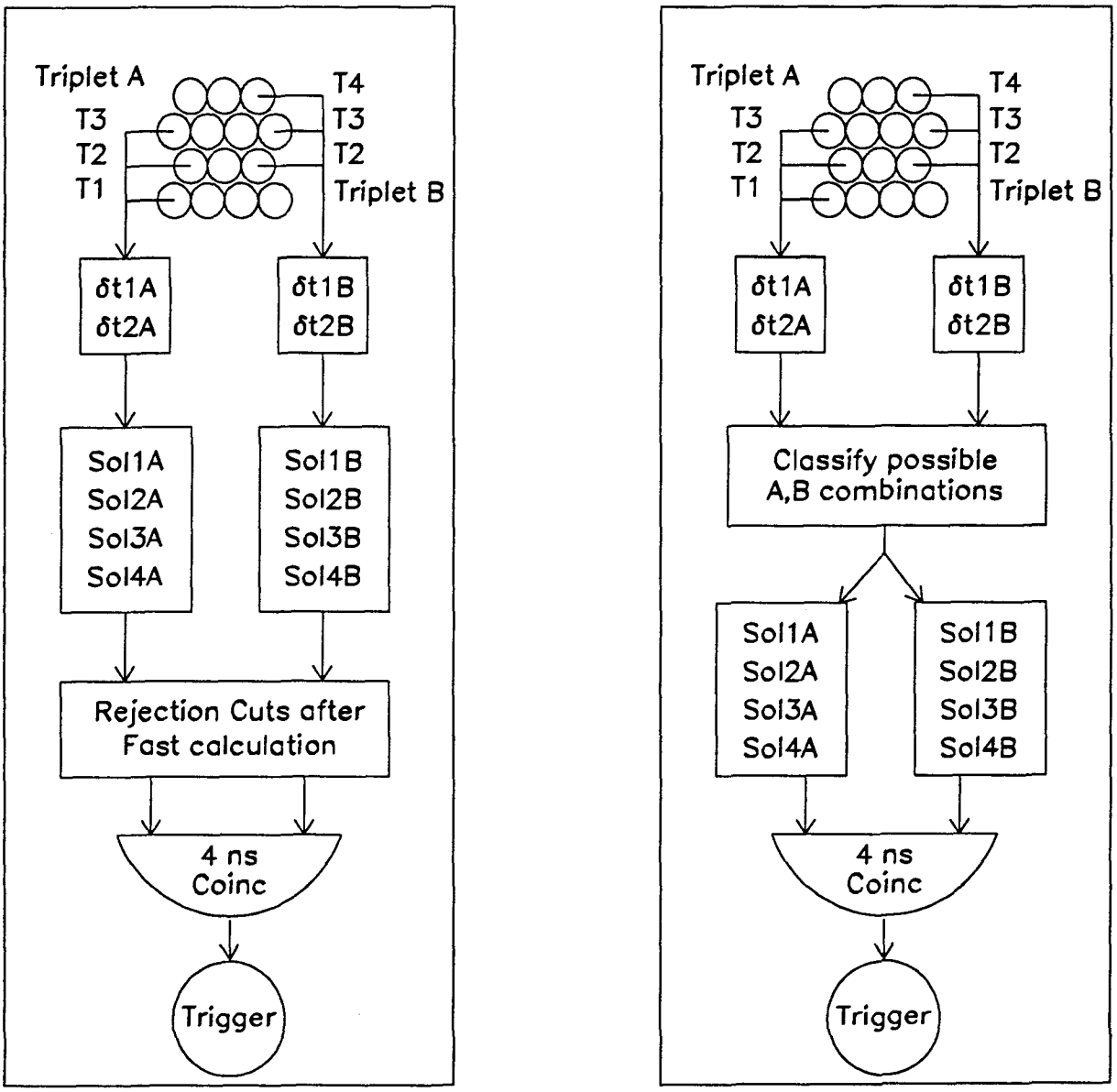

Figure 10: Rejection of early false trigger signals (ghost triggers). (a) Complex OR rejection scheme, (b) Simple OR rejection scheme.

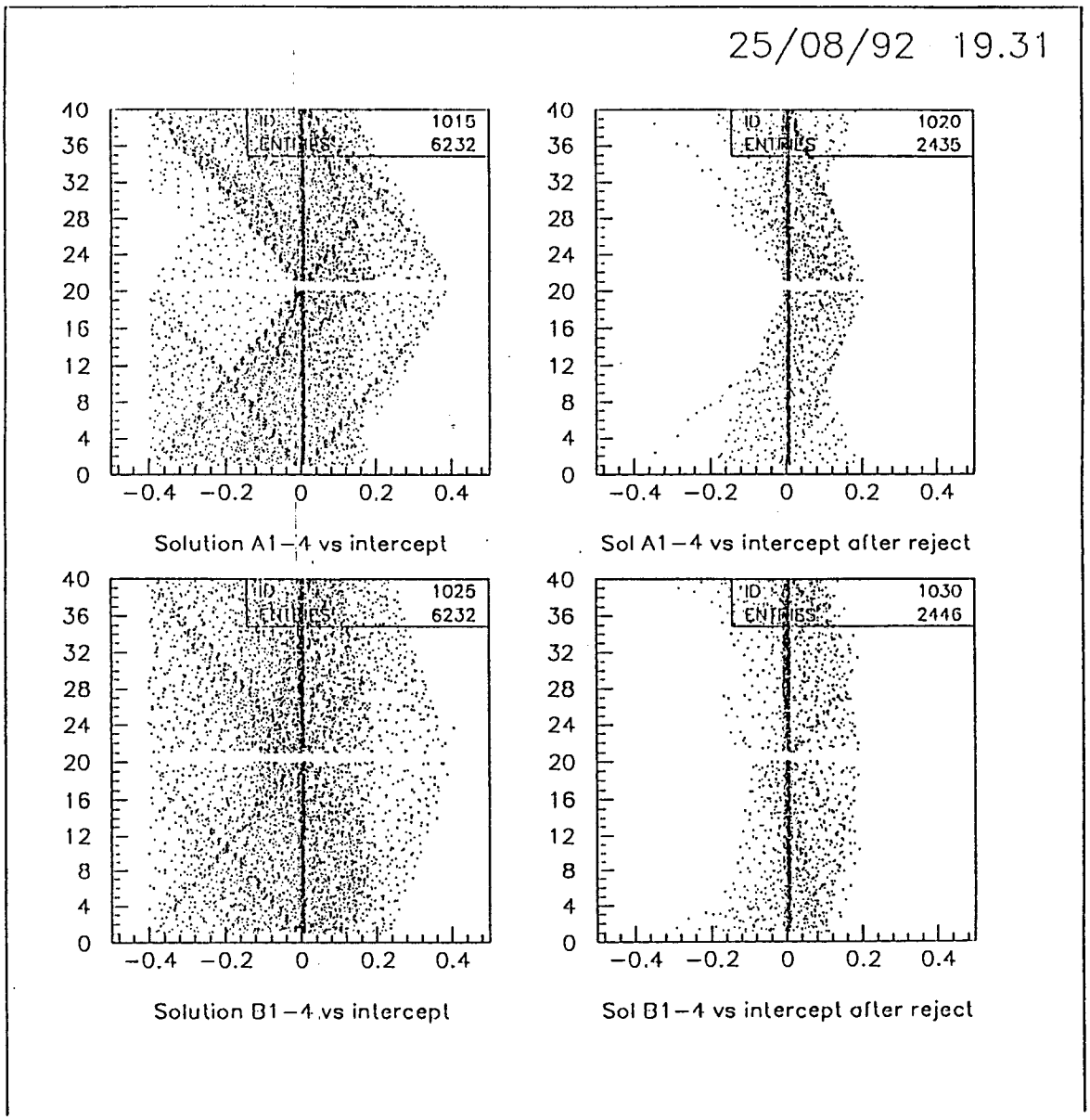

Figure 11: Simulated signals generated by the complex OR decision circuit for close packed drift tubes of 40 mm diameter as in GEM. (a) All signals from Solutions 1-4. (b) Signals from the decision circuit after rejections.

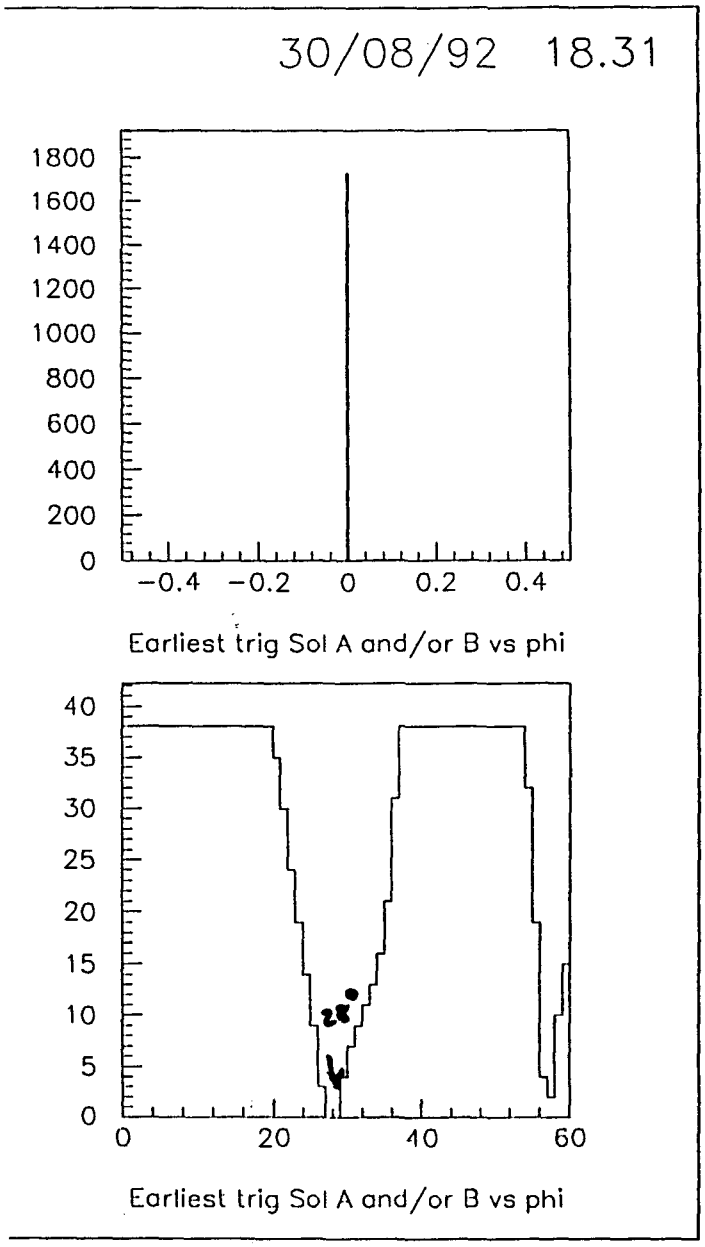

Figure 12: $\epsilon(\phi)$ Efficiency of finding a solution with a combination of triplets A.and.B, or A.or.B in the Complex OR scheme

Table 1: Filter for SolutionA + Solution B coincidences

	Condition 5*A*	*Solution* 2*A*	*Solution* 4*A*	*Solution* 1*A*	*Solution* 3*A*
Cond. 5*B*	$\delta t_{1A} + \delta t_{1B} = \frac{\delta t_{2A}}{2} + \frac{\delta t_{2B}}{2}$	$\delta t_{1A} - \delta t_{1B} = \delta t_{2A} - \delta t_{2B}$ *.AND.* $\delta t_{2A} \neq \delta t_{2B}$	$\delta t_{1A} + \delta t_{2A} = \frac{\delta t_{2B}}{2}$	Negligible	
Sol. 2*B*	$\delta t_{1A} - \delta t_{1B} = \delta t_{2A} - \delta t_{2B}$ *.AND.* $\delta t_{2A} \neq \delta t_{2B}$	Negligible	$-\delta t_{1B} = \frac{\delta t_{2A}}{2} - \frac{\delta t_{2B}}{2}$, $-\delta t_{1A} = \frac{\delta t_{2A}}{2} - \frac{\delta t_{2B}}{2}$	Negligible	
Sol. 4*B*	$\frac{\delta t_{2A}}{2} = \delta t_{1B} + \delta t_{2B}$	$\delta t_{1B} = \frac{\delta t_{2A}}{2} - \frac{\delta t_{2B}}{2}$, $\delta t_{1A} = \frac{\delta t_{2A}}{2} - \frac{\delta t_{2B}}{2}$	Negligible		
Sol. 1*B*	Negligible	Negligible		$\delta t_{2A} = \delta t_{2B}$ *.AND.* $\delta t_{1A} \neq \frac{\delta t_{2A}}{2}$	
Sol. 3*B*					$\delta t_{1A} = \frac{\delta t_{2A}}{2} + \frac{\delta t_{2B}}{2}$, $\delta t_{1B} = \frac{\delta t_{2A}}{2} + \frac{\delta t_{2B}}{2}$

these conditions describe a straight line through the four drift layers. The simple OR filter routes its output signals to the appropriate circuits for the fast calculation of the solutions. A strong advantage of using simple cuts to filter the signals is that when a pair consisting of a non-degenerate solution together with a degenerate condition is identified, (i.e. 0A+1B, 4A+0B, etc.) the correct crossing time T_0 can be obtained immediately from the non-degenerate solution without incurring a risk of false triggers.

Table 1 shows a partial filter for the (A,B) solutions, and Table 2 shows the efficiency. In Table 2 the first number given is the number of true pairs from the simulation, the second number is the number of pairs passed by the cut.

Table 2: Acceptance for SolA SolB coincidence filter

	Condition 5A	Solution 2A	Solution 4A	Solution 1A	Solution 3A
Cond.5B	1863 $\Longrightarrow$ 1852	188 $\Longrightarrow$ 388†	290 $\Longrightarrow$ 284	*Negligible*	
Sol.2B	174 $\Longrightarrow$ 388†	*Negligible*	488 $\Longrightarrow$ 480	*Negligible*	
Sol. 4B	290 $\Longrightarrow$ 278	462 $\Longrightarrow$ 460 462 $\Longrightarrow$ 462	Negligible		
Sol.1B	*Negligible*	*Negligible*		1580 $\Longrightarrow$ 1580	
Sol. 3B					924 $\Longrightarrow$ 946 924 $\Longrightarrow$ 946

† (2A+5B) and (5A+2B) are not differentiated by this cut.

4 Additional superlayers

The coincidence schemes discussed so far involve two overlapping triplets in a single superlayer. Such a scenario demands very high efficiency in all four signal layers. If we allow coincidences between triplets from different superlayers, the requirement of near 100% efficiency in each layer can be relaxed.

Ignoring the effects of multiple scattering, a high p_t track which passes through the two superlayers BW2 and BW3 is constrained to have the same slope. A trigger would require that a solution be found in either superlayer, and that the slope be the same in both superlayers. A straight track which generates hits in three out of four layers will satisfy at least one of the drift time symmetry conditions (Eqns. 2, 8-10) and can operate as a checksum of the muon system electronics [5]. However, to distinguish a high p_t track from a low p_t track which crosses between the drift wire positions, it is necessary to also satisfy one of the solutions for the crossing time (Eqns. 3-6).

The geometrical effect of coincidences between superlayers will be a topic of future investigation. In particular, the effect of the relative placement of superlayers on the size of the "holes" in the solutions will be of interest. It should be noted that, at the critical

angle ϕ_c the degenerate condition holds for all values Y of the coordinates, and this means cannot be used for its timing calculation.

5 Non-contiguous triplets

Allowing coincidences between contiguous triplets in different superlayers or with an optional trigger counter still requires disproportionately higher efficiencies in the internal layers W2 and W3. It therefore becomes necessary to investigate the solutions of the non-contiguous triplet combinations (W1,W2,W4) and (W1,W3,W4), triplets C and D respectively.

The drift time symmetry relations for these two combinations are:

$$\text{Triplet C}: \quad T_{\text{tot}} = \frac{(3T_2 - T_4)}{2} + T_1, \tag{9}$$

and

$$\text{Triplet D}: \quad T_{\text{tot}} = \frac{(3T_3 - T_1)}{2} + T_4, \tag{10}$$

If we use the definitions

$$\delta t_{1c} = |T_1 - \max(T_2, T_4)| \quad \text{and} \quad \delta t_{2c} = |T_2 - T_4| \tag{11}$$

and

$$\delta t_{1d} = |T_4 - \max(T_1, T_3)| \quad \text{and} \quad \delta t_{2d} = |T_1 - T_3|, \tag{12}$$

we can find a complete set of equations and degeneracy conditions.

$$X = \tfrac{1}{3}\left[T_{tot} - \left(\delta t_1 + \tfrac{\delta t_2}{2}\right)\right] \implies T_{tot} = \delta t_1 + \frac{\delta t_2}{2} \tag{13}$$

$$X = \tfrac{2}{3}\left[T_{tot} - \left(\delta t_1 + \tfrac{3\delta t_2}{4}\right)\right] \implies \textit{No degeneracy} \tag{14}$$

$$X = \tfrac{1}{2}\left[T_{tot} - \left(\delta t_1 - \tfrac{\delta t_2}{2}\right)\right] \implies \textit{No degeneracy} \tag{15}$$

$$X = -\tfrac{1}{2}\left(\delta t_1 - \tfrac{\delta t_2}{2}\right) \implies \delta t_1 = \frac{\delta t_2}{2} \tag{16}$$

$$X = \delta t_1 - \tfrac{\delta t_2}{2} \tag{17}$$

$$X = \tfrac{1}{3}\left[T_{tot} - \left(2\delta t_1 + \tfrac{\delta t_2}{2}\right)\right] \implies \textit{No degeneracy} \tag{18}$$

$$X = \left[T_{tot} - \left(2\delta t_1 + \tfrac{\delta t_2}{2}\right)\right] \tag{19}$$

$$X = \tfrac{1}{3}\left[T_{tot} - \left(2\delta t_1 + \tfrac{3\delta t_2}{2}\right)\right] \implies \textit{No degeneracy} \tag{20}$$

$$X = T_{tot} - \left(2\delta t_1 + \tfrac{3\delta t_2}{2}\right) \tag{21}$$

$$X = \tfrac{1}{2}\left[T_{tot} - \left(\delta t_1 + \tfrac{3\delta t_2}{2}\right)\right] \implies T_{tot} = \delta t_1 + \frac{3\delta t_2}{2} \tag{22}$$

$$X = \tfrac{1}{3}\left[T_{tot} - \left(\delta t_1 + \tfrac{3\delta t_2}{2}\right)\right] \tag{23}$$

$$X = \tfrac{1}{2}\left[2T_{tot} - \left(\delta t_1 + \tfrac{3\delta t_2}{2}\right)\right] \implies \textit{No degeneracy} \tag{24}$$

$$X = \tfrac{1}{3}\left[2T_{tot} - \left(\delta t_1 + \tfrac{3\delta t_2}{2}\right)\right] \tag{25}$$

$$X = \tfrac{1}{2}\left[T_{tot} + \left(\delta t_1 - \tfrac{3\delta t_2}{2}\right)\right] \tag{26}$$

$$X = T_{tot} + \left(\delta t_1 - \tfrac{3\delta t_2}{2}\right) \implies T_{tot} = -\delta t_1 + \frac{3\delta t_2}{2} \tag{27}$$

$$X = \delta t_1 - \tfrac{3\delta t_2}{2} \implies \delta t_1 = \frac{3\delta t_2}{2} \tag{28}$$

Figure 13 shows parameter space plots of the overall solutions and degeneracy conditions for the non-contiguous triplets. The rather large number of equations for these non-contiguous triplets precludes a straightforward implementation of the methods that were employed in the contiguous triplets. This problem will be examined in detail in a separate note.

6 SDC Muon Trigger

The first objective for our trigger scheme is to operate with a time resolution that can identify a 60 MHz beam crossing, at an SDC Level 1 trigger rate of 100 kHz. The second objective of our trigger scheme is to obtain a rough momentum measurement.

6.1 Timing

Within an projective angular range of ± 16 deg, a 4 ns wide coincidence of Solution A with Solution B gives T_0 with the required precision. The two triplet coincidence makes possible

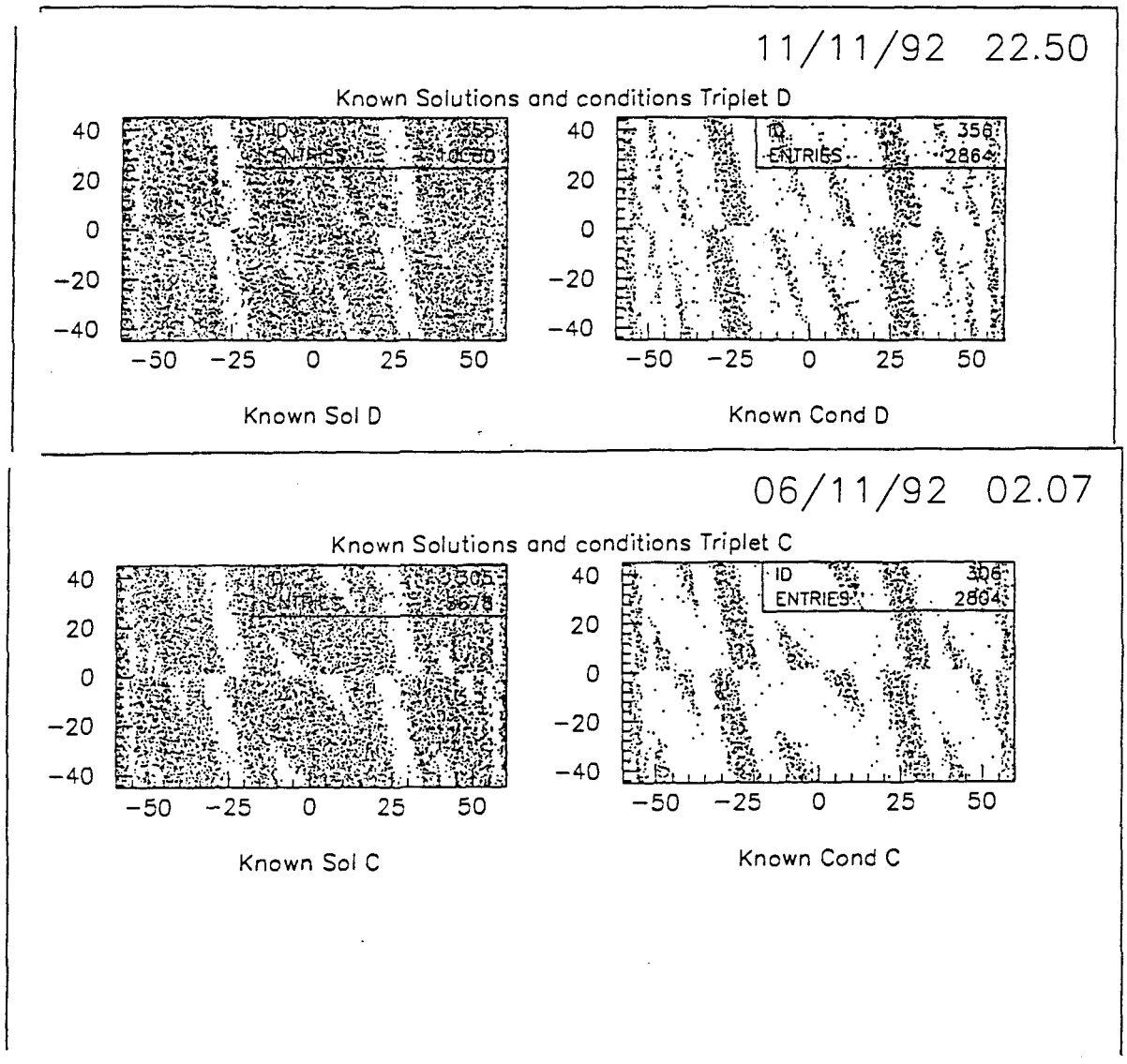

Figure 13: Solutions for Triplets C,D

a high resolution standalone timing circuit without the use of trigger scintillators. For the geometry used in this study, this proposed trigger would operate in the range between $\phi_{H1} = -16\,\mathrm{deg}$ and $\phi_{H2} = +16\,\mathrm{deg}$.

When only one triplet has a valid solution, the situation is more complex. When there is a valid solution in one triplet and a degeneracy condition in the other triplet, then if the low-level filter (simple OR cuts) has been applied, the timing can be taken from the non-degenerate solution. Otherwise when $\phi \neq \phi_c$, we must seek coincidences with a different superlayer. At any fixed angle, the probability of finding a nondegenerate solution depends on the value of Y in the other superlayer, with a total probability of 50% over the angular range of the degeneracy. The layer separation distance and relative tube offsets may affect the shape of the probability distribution which would otherwise be symmetric about ϕ_c.

When degeneracy conditions exist in both triplets, the output from the coincidence circuit can be used to block false triggers. The angular boundaries of this region are $18° \sim 33°$ for SDC and $21° \sim 36°$ for GEM. Momentum and angle information are still available if timing can be taken from an optional trigger counter.

6.2 Momentum

At transverse momenta of 5 GeV/c or higher, muons can pass through the calorimeter, BW1, the barrel toroid, BW2 and BW3 to reach the muon scintillators. For the barrel toroid system, we use a 1.8 Tesla iron toroid of 1.5 m thickness and bending power given by [2]

$$\theta = 810mr/P_t \tag{29}$$

Applying a lower limit of 5-10 GeV/c to this equation, we obtain 9.3 deg - 4.6 deg, respectively, for the maximum bend angle of a track from the interaction point. Since the muon tubes are oriented projectively, Solution 2 and the degenerate condition, whose ranges of validity begins at 12 degrees 14 degrees, respectively, may in principle be excluded from the logic of the fast calculations (thereby simplifying the electronics). In the angular range $-11° < \phi < +11°$, which corresponds to muon tracks with transverse momentum of 4.2 GeV/c or higher, the geometrical acceptance using only Solutions 1, 3 and 4, is 100%. The momentum smearing effects from multiple scattering and the finite size of the interaction region must also be considered.

7 Summary and Future Work

The close packed geometry we have used is a reasonable approximation to the spacing scheme for the central sector which spans $\eta = 0$ in the BW2 and BW3 layers. Interlayer staggering, relative placement of different superlayers and other geometrical issues should be studied in the context of this scheme. Sparcification in the outer sectors which will

impose some spatial separation between adjacent tubes in a layer will no doubt affect the total acceptance.

Table 3 lists the angular ranges of the solutions and degeneracies for Triplets A and B. The efficiency of this suggested trigger scheme near the critical angles (27° for SDC and

Table 3: Angular ranges for Triplets A and B

	Critical Angle	Degeneracy in A (or B)	Degeneracy in A and B	Sol 1	Sol 2	Sol 3	Sol 4
SDC	27°	14° ~ 36°	18° ~ 33°	−13° ~ 13°	11° ~ 26°	1° ~ 26°	1° ~ 25°
GEM	30°	16° ~ 40°	21° ~ 36°	−16° ~ 16°	12° ~ 26°	1° ~ 28°	1° ~ 28°

30° for GEM) may be increased by using a superlayer without shifts of tubes. The critical angle for such a superlayer equals zero, and the overlapping coverage could eliminate the "holes" in the acceptance of the trigger system. In principle, the necessity for such a step can be determined after considering the angular distributions of secondary background particles in more detailed simulations.

A single track version of a Level 1 trigger scheme has been described in this note. We investigated its features and the efficiency of the proposed method in the absence of background processes. Contamination from the electromagnetic debris that accompanies high energy muons will decrease the efficiency of any one track scheme, independently of the muon rate. In light of the issue of neutron fluences and beampipe activation, particularly in the forward region, an investigation of multi-hit trigger schemes will be of critical importance. Since the drift tubes which are used in the SDC muon system are multi-hit detectors, we propose to extend the present study to a multi-hit trigger scheme as the next major step of this investigation.

8 Acknowledgements

I wish to thank S. Kunori, Y. Fisyak, P. Dingus, V. Kubarovsky, P. Schuler, H. Lubatti, T. Zhao, P. McBride, T. Fukui, N. Khalatyan, G. Feldman, C. Rosenfeld and R. Hubbard for helpful suggestions, and L. Barabash for the initial ideas and discussions.

References

[1] L. Barabash, et al., *Generation of a Precisely Timed Muon Trigger Using Signals from the GEM Drift Tubes*, GEM TN-92-161, 1992

[2] T. Zhao, *An Approach of Triggering Using Drift Chambers*, SDC-91-00024, 1990

[3] Tianchi Zhao and Zhong Jin, *Level 1 Muon Trigger Simulations*, SDC-92-177

[4] A. Simon, *SDC Muon Trigger*, SDC-91-00020, 1991

[5] H. Sakamoto, Proceedings of the KEK Collaboration Meeting May 13-17, SDC-91-00033

[6] T.Groski, J.Lackey and W.H. Smith, *Correlated Level 1 Muon Trigger Design for the SDC*, SDC-91-141, 1991